Journal of Computational Physics **158,** 139–160 (2000)
doi:10.1006/jcph.1999.6405, available online at http://www.idealibrary.com on IDEAL®

A Novel Lattice BGK Approach for Low Mach Number Combustion

Olga Filippova and Dieter Hänel

Institute of Combustion and Gasdynamics, University of Duisburg, D-47048 Duisburg, Germany
E-mail: haenel@vug.uni-duisburg.de

Received April 5, 1999; revised October 25, 1999

An extended lattice Boltzmann (BGK) model is presented for the simulation of low Mach number flows with significant density changes. For applications to reactive flows this new model is coupled with a finite-difference scheme for solving the transport equations of energy and species. With a boundary fitting formulation and local grid refinement the scheme enables accurate and efficient computations of low Mach number reactive flows in complex geometry on the simplest Cartesian grids. Examples of reactive flows around porous burners are presented.

Key Words: lattice-BGK model; low Mach number flows.

1. INTRODUCTION

The computation of reactive flows requires in many cases methods able to deal with flows at low Mach numbers but significant density changes caused by heat release in chemical reactions. In general these flows are described by the whole system of Navier–Stokes equations with chemical source terms coupled with the transport equations for species. This set of equations contains entropy, vorticity, and acoustic modes [1], which in the case of low Mach number flows are of very different frequencies. If only steady-state flows and flows in the low-frequency limit (with characteristic times one order higher than characteristic time of acoustic waves propagation) are of interest then a numerical solution procedure of the whole system of equations for compressible flow becomes non-efficient or does not converge since the resolution of the acoustic fluctuations requires very small time steps. To overcome this difficulty the low Mach number approximation (LMNA) of Navier–Stokes equations was proposed in [2–4] and by others. In this reduced system of governing equations the acoustic waves are filtered out which allows us to avoid the severe restriction on the time step.

In absence of temperature gradients the low Mach number approximation of Navier–Stokes equations reduces to the system of Navier–Stokes equations for incompressible flow.

0021-9991/00 $35.00

So the methods of solution are usually extensions of methods developed for the solution of incompressible flows. Pressure relaxation methods [5] widely used for the computations of slow combustion include the solution of a Poisson equation for the pressure at each time step, which needs iteration procedures.

Recently a new class of incompressible solvers, the lattice Boltzmann methods [6, 7], here used with the collision term of the Bhatnagar–Gross–Krook (BGK) form [8–11], called lattice BGK (LBGK) methods, are created on the basis of gas-kinetic representation of fluid flow. These schemes don't deal with the discretized system of Navier–Stokes equations, but describe the evolution of discrete distribution functions in the form of relaxation equations. Hydrodynamic variables are moments of the discrete distribution functions. It can be shown that LBGK schemes provide solutions of Navier–Stokes equations for incompressible flows with second-order accuracy in Knudsen number for flows in the limit of low frequencies. With improvements as boundary fitting formulation [12], local grid refinement [12], and with acceleration in time on refined grids [13] the scheme has become competitive with well established methods for solving the Navier–Stokes equations.

The idea to extend lattice Boltzmann schemes to the solution of combustion problems belongs to Succi *et al*. [14]. In the limiting case of infinite fast reactions and "cold" flames with weak heat release the authors have described the reactive flow dynamics in two dimensions with the 24 speeds LBE-FCHC scheme including two passive scalars as mixture fraction of the fuel and temperature. As it was mentioned in [14] the next class of problems to be addressed is reacting flows at low Mach numbers in which density is allowed to respond to temperature changes over a significant dynamical range of values. The first scheme of this kind dealing with the whole system of LMNA equations in the case of simplified chemistry was proposed by the authors in [15]. It contained the modified LBGK model for solution of continuity and momentum equations and a finite-difference method for the transport equations of temperature and species. With this scheme reactive flows in a wide region of Damköhler numbers were considered.

An improved variant of this scheme is proposed in this paper which simplifies the introduction of embedded grids in zones of chemical reactions and makes the whole algorithm more stable and efficient. The modification introduces a new set of moments and additional terms in the expression for equilibrium distribution function. An interesting aspect of both schemes is that the value of the dynamic part of the pressure is not obtained explicitly during the computations. It is included together with divergences of velocity and mixture flux in the value of zero-order moment of distribution functions. To obtain the value of pressure explicitly one must apply the usual finite-difference technique to this moment.

The locality in the definition of pressure allows the use of different time-stepping in the zones of reactions and in zones of pure transport which results in a more efficient resolution of reactive flows.

The paper is organized as follows. In Section 2 the system of equations of the low Mach number approximation (LMNA) of the Navier–Stokes equations is repeated for completeness. In Section 3 the basic LBGK model for the simulation of incompressible flows is briefly presented. The modified LBGK model for the solution of continuity and momentum equations of the LMNA is described in Section 4. In Section 5 the algorithm of the combined LBGK and finite-difference scheme is presented. In Section 6 the use of the local grid refinement (embedded grids) and boundary fitting formulation are discussed in application to the new LBGK scheme. In Subsection 7.1 the results obtained with the present scheme are compared to that of a pressure relaxation method for a common test problem.

In Subsection 7.2 a few numerical examples of steady and unsteady reactive flows are presented.

2. LOW MACH NUMBER APPROXIMATION OF THE NAVIER–STOKES EQUATIONS (LMNA)

Reactive flows at low speeds are characterized by low Mach numbers but with significant changes of the density due to temperature changes by chemical reactions. In many cases the acoustic influence on reaction problems is not of interest, so the fast acoustic modes, fast compared to the convective speed, are filtered out by a low Mach number approximation (LMNA) of the Navier–Stokes equations of a compressible fluid. The approximations accounts only for changes at low frequencies with characteristic times in the order of L/U_0, where U_0 is a typical flow velocity.

The LMNA equations are derived from the full set of conservation equations for mass, momentum, energy and mass fractions of species by expanding the normalized variables $(\mathbf{u}, p, h)$ in a series of square Mach numbers $Ma^2 \ll 1$ and neglecting terms of second order in Mach number compared to dominant terms [2–4]. The low Mach number approximation of Navier–Stokes equations (LMNA) together with the transport equations for the species results in the following system of equations,

$$\partial_t \rho_{mix} + \partial_\alpha(\rho_{mix} u_\alpha) = 0 \tag{1}$$

$$\partial_t \rho_{mix} u_\alpha + \partial_\beta(\rho_{mix} u_\beta u_\alpha) + \partial_\alpha p^{(1)} - \partial_\beta \mu\left(\partial_\beta u_\alpha + \partial_\alpha u_\beta - \frac{2}{3}\delta_{\alpha\beta}\partial_\gamma u_\gamma\right) = 0 \tag{2}$$

$$\rho_{mix} C_p(\partial_t T + u_\beta \partial_\beta T) = \partial_\gamma C_p \chi \rho_{mix} \partial_\gamma T + \sum_i h_i w_i - \nabla \rho_{mix} T \sum_i C_{p,i} \xi_i \mathbf{V}_i + \frac{\partial p^{(0)}}{\partial t} \tag{3}$$

$$\partial_t \xi_i + u_\beta \partial_\beta \xi_i = \frac{1}{\rho_{mix}} \partial_\gamma D_i \rho_{mix} \partial_\gamma \xi_i + \frac{w_i}{\rho_{mix}}, \qquad \sum_i \xi_i = 1, \quad i = 1, \ldots, N \tag{4}$$

$$p^{(0)} = \rho_{mix} RT = p^{(0)}(t), \tag{5}$$

where ρ_{mix} and $\mathbf{u}$ are the density and velocity of the mixture, μ is dynamic viscosity, χ is the coefficient of thermal diffusivity, and C_p is the constant pressure specific heat capacity of the mixture. In addition, ξ_i, $\mathbf{V}_i$ are the mass fraction and diffusion velocity of ith species, D_i is the diffusivity of ith species in the mixture, $C_{p,i}$ is the constant pressure specific heat capacity, and w_i and h_i are the rate of production and heat of formation of the ith species, respectively.

The pressure splits in two parts: in a thermodynamic part $p^{(0)}(t)$ which is constant in an open system and in a hydrodynamic part $p^{(1)}(t, \mathbf{r})$ associated with the gas motion. The fact that the thermodynamic part of the pressure is constant in an open system results in the following algebraic relationship for a mixture containing N species with different molecular weights W_i,

$$\rho_{mix} T a = \rho_0 T_0 a_0, \qquad a = \sum_{i=1}^{N} \frac{\xi_i}{W_i}.$$

Here and below the reference values ρ_0, T_0, a_0 denote the density, the temperature, and the molar density of the mixture.

3. BASIC LATTICE BGK APPROACH

The lattice Boltzmann method [6, 7] and its recent modification, the lattice-BGK (LBGK) [8–11] method, provide kinetic concepts for simulating incompressible, continuum flows, described by the Navier–Stokes equations. The "isothermal" LBGK models are mostly used for incompressible flows and will be explained briefly as the basis for the solution of LMNA equations.

The computational method is based on the development of discrete molecular velocity distribution functions f_{pi} on uniform Cartesian lattices with additional diagonal links [8, 9],

$$f_{pi}(t+\delta_t, \mathbf{r}+\mathbf{c}_{pi}\delta_t) = f_{pi}(t,\mathbf{r}) + \omega\big[f_{pi}^{\mathrm{eq}}(t,\mathbf{r}) - f_{pi}(t,\mathbf{r})\big]. \tag{6}$$

The index i defines the vector of the discrete molecular velocities and the index p is the square modulus of the corresponding molecular velocity $\mathbf{c}_{pi}$ [8]. The most commonly used LBGK model in 2D deals with 9 discrete molecular velocities with components $(c_0, 0)$, (c_0, c_0), $(0, c_0)$, $(-c_0, c_0)$, $(-c_0, 0)$, $(-c_0, -c_0)$, $(0, -c_0)$, $(c_0, -c_0)$, and $(0, 0)$. The equilibrium distribution function f_{pi}^{eq} is a discrete analog of the Maxwellian distribution function expanded for small Mach numbers [8, 9]. For incompressible flows with a density $\rho_0 = 1$ one can take it in the form [10, 11]

$$f_{pi}^{\mathrm{eq}} = t_p\left[\frac{p}{\rho_0 c_s^2} + \frac{u_\alpha c_{pi\alpha}}{c_s^2} + \frac{u_\alpha u_\beta}{2c_s^2}\cdot\left(\frac{c_{pi\alpha}c_{pi\beta}}{c_s^2} - \delta_{\alpha\beta}\right)\right], \tag{7}$$

where the t_p are weighting coefficients, δ_x is the lattice spacing, $c_0 = \delta_x/\delta_t$ is the Cartesian component of molecular velocity for moving molecules, and $c_s = c_0/\sqrt{3}$ is the speed of sound in this molecular system.

The macroscopic flow variables are computed on each node as moments of the discrete distribution functions

$$p = \rho_0 c_s^2 \sum_{p,i} f_{pi}, \qquad \mathbf{u} = \sum_{p,i} f_{pi}\mathbf{c}_{pi}. \tag{8}$$

The two essential parameters of the LBGK method are the Knudsen number ϵ and the global Mach number M_g. Both are values much less than one. The Knudsen number of the system $\epsilon = \delta_x/L$ is defined as the ratio between lattice spacing δ_x and characteristic length of the flow L. The characteristic length L is defined as the characteristic distance on which hydrodynamic variables are essentially changing, as, for example, over the thickness of a boundary layer. The geometrical length, typically a body length, is designed as L_0. In nearly isotropic flows the characteristic length is $L \sim L_0$, but in cases of strongly anisotropic flows where zones are resolved on grids with different lattice spacings one has to differ between L and L_0 [13]. The Mach number is introduced as the global Mach number $M_g = U_0/c_0$ which is the ratio of a characteristic velocity U_0 of the flow and the molecular speed c_0 on the lattice. The derivation of the macrodynamical equations from the LBGK equations using multi-scales asymptotics is described in detail in [11, 16]. This derivation is essentially based on Chapman–Enskog and Taylor expansions in two different characteristic times of the flow, the characteristic time of acoustic waves propagation ($T_1 \sim \epsilon^{-1}\delta_t$), and the characteristic time of low frequency hydrodynamics ($T_2 \sim \epsilon^{-2}\delta_t$). Using expansion of

the distribution function around the local equilibrium state in a series of small parameter $\delta_t = \epsilon L/c_0$ and the symmetry properties of the lattice one can obtain the following system of macrodynamical equations [11],

$$\frac{\partial p}{\rho_0 c_s^2 \partial t} + \partial_\alpha u_\alpha = 0 \tag{9}$$

$$\rho_0 \left(\frac{\partial u_\alpha}{\partial t} + u_\beta \partial_\beta u_\alpha \right) = -\partial_\beta p \delta_{\alpha\beta} + \mu \Delta u_\alpha + O\big(M_g^3\big). \tag{10}$$

The resulting kinematic viscosity $\nu = \mu/\rho_0$ is related to the relaxation parameter ω by the formulation [11]

$$\nu = \frac{\delta_x c_0}{6} \left(\frac{2}{\omega} - 1 \right). \tag{11}$$

When acoustic time scales exist in the solution the scheme can be considered as a "weak-compressible" isothermal solver according to macrodynamical equations Eqs. (9)–(10). However, if the external conditions are uniform in time then acoustic fluctuations usually introduced in the LBGK scheme by initial conditions dissipate relatively fast. Then the resulting flow field is governed by the low frequency solution with a characteristic time of $T \sim (M_g \epsilon)^{-1} \delta_t$. The characteristic time T corresponds to a range of Strouhal numbers of

$$Str = \frac{L_0}{U_0 T} = \frac{\delta_t}{T M_g \epsilon} \sim O(1)$$

and is consistent with the range obtained experimentally, e.g., for vortex streets. This behaviour was confirmed by the large amount of numerical experiments [12, 16, 17]. Based on this experience the analysis for deriving the macroscopic equations from the LBGK approach can be simplified if only characteristic time scales of order T are of interest. The analysis performs in a similar way using Chapman–Enskog and Taylor expansions but with respect to one time scale only. It was shown in [13] that the macrodynamical equations derived with the one-scale approach approximate the Navier–Stokes equations for incompressible flow with second order accuracy $O(\epsilon^2)$, if Mach number and Knudsen number are of the same order of magnitude, $M_g \sim \epsilon$.

In the following discussion of LBGK methods for the LMNA equations the resulting macrodynamics is considered in the limit of low frequencies ($T \sim (M_g \epsilon)^{-1} \delta_t$) only. The transitional regime from the start of computations up to obtaining the low frequency limit is not analyzed.

4. LATTICE BGK APPROACH FOR FLOWS WITH VARIABLE DENSITY (LMNA)

The system of continuity equation, Eq. (1), and momentum equation, Eq. (2), of the LMNA has similar properties as the corresponding equations for incompressible flows. The pressure $p^{(1)}$ acts like a parameter to satisfy the continuity equation. In usual Navier–Stokes solvers the pressure is calculated iteratively from a Poisson equation derived from the divergence of the momentum equations. In LBGK methods for incompressible flows the pressure-velocity coupling is included in the relaxation procedure of the distribution function and acts macroscopically like a weak-compressible solver. Effects of compressibility

become negligible in low-frequency limit and the LBGK scheme performs macroscopically as an incompressible solver with second order accuracy in Knudsen number. Thus the LBGK concept for incompressible flow [10, 11] can be transferred to the LMNA equations. An essential difference between both is the variable density $\rho_{mix}(T, a)$. But, if the energy and species equations are considered to be decoupled during a time step, the density becomes an external quantity as a function of temperature and molar density of the mixture in the system of continuity and momentum equations.

In consequence, the LBGK approach for incompressible flows can be used for the system of continuity equation, Eq. (1), and momentum equation, Eq. (2) of LMNA equations but with suited modifications to take into account the temporal and spatial variation of density $\rho_{mix}(T)$ and to ensure the same numerical accuracy.

The modifications of the lattice BGK method for low Mach number flows with variable density are described in the following.

For links with finite molecular velocities ($p \neq 0$) the rate equation for the distribution function is unchanged,

$$f_{pi}(t + \delta_t, \mathbf{r} + \mathbf{c}_{pi}\delta_t) = f_{pi}(t, \mathbf{r}) + \omega\big[f_{pi}^{\mathrm{eq}}(t, \mathbf{r}) - f_{pi}(t, \mathbf{r})\big], \qquad p \neq 0. \tag{12}$$

For resting molecules ($p = 0$) it is

$$f_0(t + \delta_t, \mathbf{r}) = f_0(t, \mathbf{r}) + \omega\big[f_0^{\mathrm{eq}}(t, \mathbf{r}) - f_0(t, \mathbf{r})\big] - G(t, \mathbf{r}), \qquad p = 0. \tag{13}$$

The additional factor G models the temporal change of the density $\rho_{mix}(t, \mathbf{r})$

$$G(t, \boldsymbol{r}) = \frac{\rho_{mix}(t, \mathbf{r})}{\rho_0} - \frac{\rho_{mix}(t - \delta_t, \mathbf{r})}{\rho_0}.$$

For the computations of steady-state problems the term $G(t, \mathbf{r})$ in Eq. (13) can be omitted. The equilibrium distribution function f_{pi}^{eq} is changed in the following way:

$$\begin{aligned} f_{pi}^{\mathrm{eq}}(t, \mathbf{r}) = \frac{t_p}{\rho_0}\Bigg[& \frac{P(t, \mathbf{r})}{c_s^2} + \frac{\rho_{mix}(t, \mathbf{r})u_\alpha(t, \mathbf{r})c_{pi\alpha}}{c_s^2} \\ & + \frac{\rho_{mix}(t, \mathbf{r})u_\alpha(t, \mathbf{r})u_\beta(t, \mathbf{r})}{2c_s^2}\left(\frac{c_{pi\alpha}c_{pi\beta}}{c_s^2} - \delta_{\alpha\beta}\right) \\ & + \frac{\nu(t, \mathbf{r})u_\gamma(t, \mathbf{r})\partial_\delta\rho_{mix}(t, \mathbf{r})}{c_s^2}\left(\frac{c_{pi\gamma}c_{pi\delta}}{c_s^2} - \delta_{\gamma\delta}\right)\Bigg]. \end{aligned} \tag{14}$$

The new formulation of the effective equilibrium distribution function takes into account the variable density and changes the meaning of the moments.

The zeroth moment results in a pressure-like term P

$$P(t, \mathbf{r}) = \rho_0 c_s^2 \sum_{p,i} f_{pi}(t, \mathbf{r}) = p^{(1)} + \frac{2}{3}\mu\partial_\gamma u_\gamma + \nu\partial_\gamma\rho_{mix}u_\gamma. \tag{15}$$

The term P, containing macroscopically the dynamic part of pressure $p^{(1)}$ and the divergences of the velocity and the mixture flux, is defined to correct the expression for the stress tensor to its physical definition in the macrodynamical momentum equations. Its derivation is given in the Appendix.

The first moment of the discrete distribution function represents the flux of the mixture

$$\rho_{mix}\mathbf{u} = \rho_0 \sum_{p,i} f_{pi}\mathbf{c}_{pi} \tag{16}$$

instead of the velocity of the mixture as it was proposed in the previous LBGK model [15]. The kinematic viscosity ν takes into account the variable density ρ_{mix} and is connected with the relaxation parameter ω by

$$\nu = \frac{\mu(T)}{\rho_{mix}} = \frac{\mu(T)}{\rho_0 T_0 a_0} Ta = \frac{\delta_x c_0}{6}\left(\frac{2}{\omega} - 1\right). \tag{17}$$

The reference viscosity $\mu_0 = \mu(T = T_0)$ is directly related to the Reynolds number Re by

$$Re = \frac{UL\rho_0}{\mu_0}. \tag{18}$$

Notice that the relaxation parameter ω in Eq. (12) and Eq. (13) is now a field variable depending on the temperature and molar density of the mixture even if the dynamic viscosity does not depend on the temperature.

An analytical proof of consistency of the macrodynamical equations provided by this modified LBGK approach with the continuity and momentum equations of LMNA and estimation of the accuracy is given in the Appendix.

It is shown there that the macrodynamical equations provided by the LBGK scheme approximate the continuity and momentum equations Eq. (1) and Eq. (2) of the LMNA of the Navier–Stokes equations beside the truncated terms of the order $O(M_g\epsilon)$ of the dominant terms. If M_g is chosen in the same order as ϵ, i.e., $M_g \sim \epsilon \ll 1$, the solution of the continuity and momentum equations of the LMNA is approximated by the solution obtained with the LBGK model with second order accuracy in the Knudsen number $\epsilon = \delta_x/L$.

5. NUMERICAL SCHEME

The numerical algorithm is based on a coupled procedure between the solution of the LBGK method for the flow part and a finite difference solution for the transport equations for temperature and species.

If at a time t all macroscopic variables and the values of distribution functions f_{pi} are assumed to be known then the modified lattice-BGK equations Eqs. (12)–(13) can be solved for each link i

$$f_{pi}(t + \delta_t, \mathbf{r} + \mathbf{c}_{pi}\delta_t) = f_{pi}(t, \mathbf{r}) + \omega\left[f_{pi}^{\mathrm{eq}}(t, \mathbf{r}) - f_{pi}(t, \mathbf{r})\right], \qquad p \neq 0$$

and for zero molecular velocity $p = 0$

$$f_0(t + \delta_t, \mathbf{r}) = f_0(t, \mathbf{r}) + \omega\left[f_0^{\mathrm{eq}}(t, \mathbf{r}) - f_0(t, \mathbf{r})\right] - \frac{\rho_{mix}(t, \mathbf{r})}{\rho_0} + \frac{\rho_{mix}(t - \delta_t, \mathbf{r})}{\rho_0}.$$

On the new time-level $t + \delta t$ the fluxes $\rho_{mix}\mathbf{u}$ and the function P which includes dynamic pressure and divergences of velocity and flux of the mixture are obtained as moments of

the distribution functions

$$P(t+\delta_t,\mathbf{r}) = \rho_0 c_s^2 \sum_{p,i} f_{pi}(t+\delta_t,\mathbf{r}) = p^{(1)} + \frac{2}{3}\mu\partial_\gamma u_\gamma + \nu\partial_\gamma \rho_{mix} u_\gamma$$

$$\rho_{mix}\mathbf{u}(t+\delta_t,\mathbf{r}) = \rho_0 \sum_{p,i} f_{pi}(t+\delta_t,\mathbf{r})\mathbf{c}_{pi}.$$

We mention here that although the values of all hydrodynamic variables included in the expression for the zeroth moment of the distribution function do not have to be defined explicitly in the internal points of the computational domain, they have to be evaluated at the boundaries.

The convective-diffusion equations for the temperature T and the species in an open system (written here in variables $\rho_{mix}\mathbf{u}$ with assumption of the same $C_{p,i}$ for all species)

$$\partial_t T + \frac{aT(\rho_{mix}\mathbf{u})}{a_0 T_0 \rho_0}\nabla T = \frac{aT}{C_p a_0 T_0 \rho_0}\partial_\gamma C_p \chi \rho_{mix}\partial_\gamma T + \frac{aT}{C_p a_0 T_0 \rho_0}\sum_i h_i w_i$$

$$\partial_t \xi_i + \frac{aT(\rho_{mix}\mathbf{u})}{a_0 T_0 \rho_0}\nabla \xi_i = \frac{aT}{a_0 T_0 \rho_0}\partial_\gamma D_i \rho_{mix}\partial_\gamma \xi_i + \frac{aT}{a_0 T_0 \rho_0} w_i, \qquad i = 1,\ldots,N-1$$

can be integrated by any finite-difference scheme. In the computational examples presented below an explicit Euler scheme is used. Within the levels t and $t+\delta_t$ the values of fluxes are linear interpolated from the time levels t and $t+\delta_t$. Then at time $t+\delta_t$ the values of function $a(t+\delta_t,\mathbf{r}) = \sum_{i=1}^{N}(\xi_i(t+\delta_t,\mathbf{r})/W_i)$, the relaxation parameter $\omega(T(t+\delta_t,\mathbf{r}), a(t+\delta_t,\mathbf{r}))$, and the density of the mixture $\rho_{mix}(t+\delta_t,\mathbf{r}) = \rho_0 T_0 a_0/(T(t+\delta_t,\mathbf{r})a(t+\delta_t,\mathbf{r}))$ are known.

The value of the effective equilibrium distribution function is completed by

$$\begin{aligned} f_{pi}^{\mathrm{eq}}(t+\delta_t,\mathbf{r}) = \frac{t_p}{\rho_0}\Bigg(& \frac{P(t+\delta_t,\mathbf{r})}{c_s^2} + \frac{\rho_{mix}(t+\delta_t,\mathbf{r})u_\alpha(t+\delta_t,\mathbf{r})c_{pi\alpha}}{c_s^2} \\ & + \frac{\rho_{mix}(t+\delta_t,\mathbf{r})u_\alpha(t+\delta_t,\mathbf{r})u_\beta(t+\delta_t,\mathbf{r})}{2c_s^2}\left(\frac{c_{pi\alpha}c_{pi\beta}}{c_s^2} - \delta_{\alpha\beta}\right) \\ & + \frac{\nu(t+\delta_t,\mathbf{r})u_\gamma(t+\delta_t,\mathbf{r})\partial_\delta \rho_{mix}(t+\delta_t,\mathbf{r})}{c_s^2}\left(\frac{c_{pi\gamma}c_{pi\delta}}{c_s^2} - \delta_{\gamma\delta}\right)\Bigg). \end{aligned}$$

For reasons of stability the last term in the expression for the effective equilibrium distribution function is reformulated using the relation $\rho_{mix} T a = \rho_0 T_0 a_0$,

$$-\frac{t_p \mu(t+\delta_t,\mathbf{r})\rho_{mix}(t+\delta_t,\mathbf{r})u_\gamma(t+\delta_t,\mathbf{r})\partial_\delta a(t+\delta_t,\mathbf{r})T(t+\delta_t,\mathbf{r})}{\rho_0^2 a_0 T_0 c_s^2}\left(\frac{c_{pi\gamma}c_{pi\delta}}{c_s^2} - \delta_{\gamma\delta}\right).$$

The procedure is repeated on the new time-level $t = t+\delta_t$.

As one can see from this numerical algorithm the explicit expression for dynamic pressure $p^{(1)}$ in the internal points of the computational domain is not necessary for the computation of all other variables.

6. LOCAL GRID REFINEMENT AND BOUNDARY FITTING FORMULATION

The computation of low Mach number combustion in a wide region of Reynolds and Damköhler numbers requires the resolution of high anisotropic parts of the flow as boundary

layers or zones of chemical reactions. The use of an uniform, fine mesh results in an unnecessary high computational effort, which can be essentially reduced by refining locally only those zones where high resolution is required. For this purpose a local second-order grid refinement concept for LBGK models using embedded grids was proposed recently by the authors [12].

Beside the spatial refinement with factors $n = \delta_{x,coarse}/\delta_{x,fine} = O(10)$ the refinement procedure allows us to use different time steps on different grids which is especially important for combustion problems if fast reactions are considered because this kind of spatial and temporal refinement reduces the stiffness of source terms in the equations for temperature and species and enables us to solve them on the same Cartesian grid as LBGK equations in the simplest explicit manner.

The boundary fitting formulation [12] was proposed by the authors for the basic LBGK scheme for incompressible flows. They allow us to describe Dirichlet boundary conditions for velocity on arbitrary curvilinear surfaces lying between the nodes of a Cartesian grid. The boundary fitting concept can be used in the present modified LBGK model in a slightly changed form. The changes are caused by the changed form of the equilibrium distribution function and by the dependence of the relaxation parameter ω on the temperature.

A curved boundary lying between the nodes of the uniform lattice with additional diagonal links is sketched in Fig. 1. If the values of the mixture flux $\rho^g_{mix}\mathbf{u}^g$ on the boundary are known (where $\rho^g_{mix}\mathbf{u}^g \neq 0$ for porous boundaries) then the distribution function coming to the "fluid" node $\mathbf{r}_f$ from the "rigid" one $\mathbf{r}_b$ lying inside of the body is prescribed by

$$f_{pi_1}(t+\delta_t, \mathbf{r}_f) = \left[(1-\omega(t,\mathbf{r}_f))\, f_{pi}(t,\mathbf{r}_f) + \omega(t,\mathbf{r}_f)\, f^{\mathrm{eq}}_{pi}(t,\mathbf{r}_f)\right](1-\omega_i) + a_1\omega_i\, f^{\mathrm{eq}}_{pi}(t,\mathbf{r}_b) + a_2\omega_i\, f^{\mathrm{eq}}_{pi}(t,\mathbf{r}_f) - 2t_p \frac{\rho^g_{mix} u^g_\alpha c_{pi\alpha}}{\rho_0 c_s^2}, \tag{19}$$

where ω_i is an adjusting parameter, $\omega(t, \mathbf{r}_f)$ is the relaxation parameter in the "fluid" node $\mathbf{r}_f$, $\mathbf{c}_{pi_1} = -\mathbf{c}_{pi}$, and the coefficients a_1 and a_2 satisfy $a_1 \cdot a_2 = 0$ and $a_1^2 + a_2^2 = 1$. The

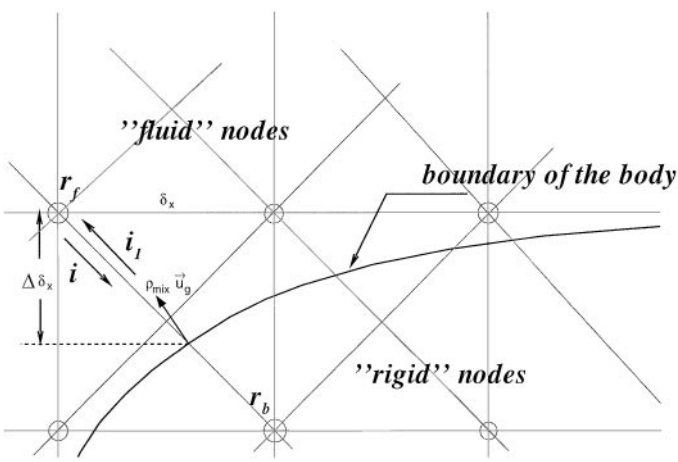

FIG. 1. Computational mesh and geometrical relations for fitting of the curvilinear boundary.

"equilibrium distribution function" in the "rigid" nodes $f_{pi}^{\mathrm{eq}}(t, \mathbf{r}_b)$ is defined as

$$f_{pi}^{\mathrm{eq}}(t, \mathbf{r}_b) = \frac{t_p}{\rho_0}\left(\frac{P(t, \mathbf{r}_f)}{c_s^2} + \frac{\rho_{mix}(t, \mathbf{r}_b) u_\alpha(t, \mathbf{r}_b) c_{pi\alpha}}{c_s^2} + \frac{\rho_{mix}(t, \mathbf{r}_f) u_\alpha(t, \mathbf{r}_f) u_\beta(t, \mathbf{r}_f)}{2c_s^2}\left(\frac{c_{pi\alpha} c_{pi\beta}}{c_s^2} - \delta_{\alpha\beta} \right) + \frac{\nu(t, \mathbf{r}_f) u_\gamma(t, \mathbf{r}_f) \partial_\delta \rho_{mix}(t, \mathbf{r}_f)}{c_s^2}\left(\frac{c_{pi\gamma} c_{pi\delta}}{c_s^2} - \delta_{\gamma\delta} \right) \right), \tag{20}$$

where $\rho_{mix}(t, \mathbf{r}_b)\mathbf{u}(t, \mathbf{r}_b)$ is the linear extrapolated value of $\rho_{mix}\mathbf{u}$ from the node $\mathbf{r}_f$ through the known value on the boundary

$$\rho_{mix}(t, \mathbf{r}_b)\mathbf{u}(t, \mathbf{r}_b) = \frac{\Delta - 1}{\Delta}\rho_{mix}(t, \mathbf{r}_f)\mathbf{u}(t, \mathbf{r}_f) + \frac{\rho_{mix}^g \mathbf{u}^g}{\Delta}.$$

Here $\Delta\delta_x$ is the Cartesian component of the distance from the node $\mathbf{r}_f$ to the boundary along the link i. The projection of flux $\rho_{mix}^g u_\alpha^g c_{pi\alpha}$ is taken in the crossing point of the boundary and the link i.

After a Taylor expansion of Eq. (19) and an expansion of the distribution function around the local equilibrium state one obtains the same relationships between ω_i and $\omega(t, \mathbf{r}_f)$ as in the case of incompressible flows [12]. For reasons of stability the following combination of boundary fitting conditions has to be used in Eq. (19):

$$\omega_i = \omega(t, \mathbf{r}_f)\,(2\Delta - 1), \qquad a_1 = 1, \quad a_2 = 0 \quad \Delta \geq 0.5 \tag{21}$$

$$\omega_i = \omega(t, \mathbf{r}_f)\frac{(2\Delta - 1)}{(1 - \omega(t, \mathbf{r}_f))}, \qquad a_1 = 0, \quad a_2 = 1 \quad \Delta < 0.5. \tag{22}$$

One has to emphasize that these simple algebraic formulas are obtained as in [12] for the case of low frequency flows with characteristic times $T \sim (M_g\epsilon)^{-1}\delta_t$ after sorting terms in the LBGK equation in the order of Knudsen number ϵ and equating the coefficient of the dominant term to zero. Neglecting of high-order in ϵ terms in the expansion series results in indistinct position of the curvilinear boundary described with the boundary fitting formulas. It is lying "somewhere" in the shell with thickness $\sim\epsilon\delta_x$ around the geometrical boundary. Nevertheless this boundary formulation is consistent with second order accuracy of the inner scheme as also estimations with Richardson's formula in [13] have confirmed. According to our experience the LBGK schemes with this kind of boundary formulation were always stable in simulation of flows around the isolated complex curvilinear geometry as cylinders, airfoils [13], grids of crossing wires with deposited particles (spheres) [18], and others if the resolution in boundary layer was reasonable ($\epsilon \sim 0.1$). However, in regions of connection with boundaries described with different kind of boundary conditions as, for example, the edges of the inlet or outlet of a channel, the LBGK scheme can become unstable [19, 20]. To our experience, this instability depends on the common discretization of the boundary conditions at the edges [21] and can be avoided by an appropriate formulation.

In the following, the boundary fitting formulas are applied to isolated curvilinear boundaries as the boundaries of the porous burners in the reactive flow.

7. NUMERICAL RESULTS

7.1. Validation of the LBGK method for reactive flows. Although several numerical approaches have been employed for the simulation of low speed reacting flows [22–25] up to now there are no sufficiently complex benchmark computations available for analysis and validation of different codes [23]. The quasi-two-dimensional benchmark problem recently proposed by Tomboulides *et al*. [23, 24] is very suitable for analyzing splitting errors in methods based on straight discretization of Navier–Stokes equations but it is not directly applicable to the lattice Boltzmann solver.

For these reasons the new scheme is validated on results obtained for a common test problem solved by a finite difference pressure relaxation method in our numerical group.

In all computational examples presented below molecular weights of all species are assumed to be the same and reference values of a_0, ρ_0, T_0 are taken as units, which results in $a = 1$ and $\rho_{mix} T = 1$. Results of computations taking into account different molecular weights of species are given in [26].

The finite difference method used for comparison is based on a pressure relaxation method. The discretization is performed on a Cartesian, non-staggered mesh with second order upwind schemes for the convective terms and central differences for the diffusive and pressure terms. The Poisson equation of pressure is solved with an overrelaxed Gauss–Seidel iteration scheme. The time integration is performed with an explicit, multi-stepping Runge–Kutta scheme, while in each time step a fractional step method [5] is used to solve the system, which proceeds in 3 steps:

$$
\begin{aligned}
\text{(Step 1)}\quad & u_\alpha^\star = u_\alpha^n - \Delta t\, \mathrm{Res}_{u_\alpha}(u^n, \rho^n) \\
& \xi_i^{n+1} = \xi_i^n - \Delta t\, \mathrm{Res}_\xi(\mathbf{u}^n, T^n, \rho^n, \xi^n) \\
& T^{n+1} = T^n - \Delta t\, \mathrm{Res}_T(\mathbf{u}^n, T^n, \rho^n, \xi^n) \\
\text{(Step 2)}\quad & \partial_\alpha\left(\frac{1}{\rho^{n+1}}\partial_\alpha\, p^{(1)}\right) = \frac{1}{\Delta t}\partial_\alpha\left(u_\alpha^{n+1} - u_\alpha^\star\right) \\
\text{(Step 3)}\quad & u_\alpha^{n+1} = u_\alpha^\star - \Delta t\, \partial_\alpha\, p^{(1)}.
\end{aligned}
$$

The common model problem describes the flow of a hot oxidizer around a periodical grid of porous burners, through which cold fuel is injected into the flow. The temperature of the oxidizer at the entrance is assumed twice the temperature of the injected fuel. The Reynolds number of the flow is $Re = 80$ related to the velocity of the oxidizer at the entrance, to the diameter of the burner, and to the viscosity in the vicinity of the burner.

In Fig. 2 the field of temperature and streamlines around the burners are shown at first for the non-reactive case with temperature changes. The velocity of injected fuel is equal to one percent of the velocity of the oxidizer at the entrance. Figure 2a presents the result obtained from the pressure relaxation method; Fig. 2b shows the results calculated with the LBGK method. The results are in very close agreement.

A reactive flow case is presented in Fig. 3 for the same geometry, but with a higher velocity of injection of 10% of the velocity of the oxidizer at the entrance. Figure 3a presents the field of temperature and streamlines of the mixture computed with the pressure relaxation method and Fig. 3b shows the corresponding values obtained with the LBGK method. The lowest and highest values of the temperature are shown in brackets.

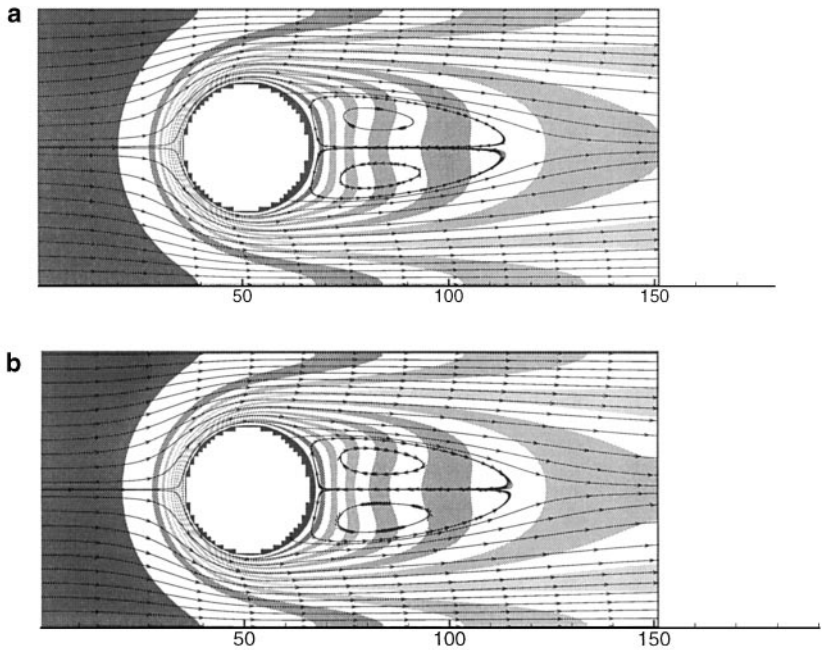

FIG. 2. Streamlines and temperature of the flow through periodical grid of porous burners at Re = 80 (no reactions), computed with the pressure relaxation method (a) and LBGK method (b). Velocity of injection is equal to 1% of velocity of the oxidizer at the entrance.

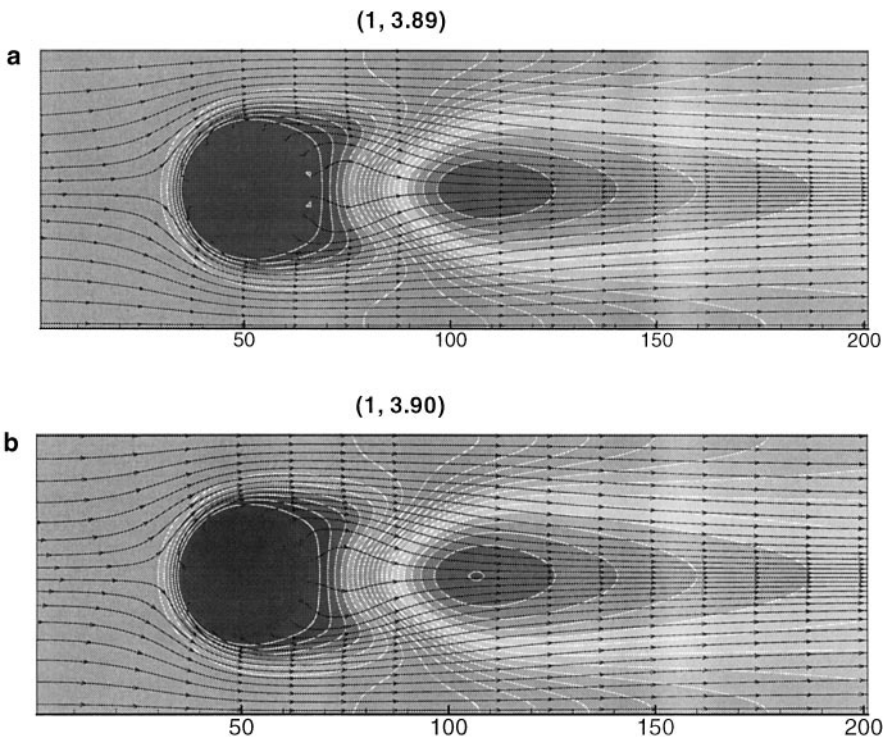

FIG. 3. Streamlines and temperature of the flow through periodical grid of porous burners at Re = 80 (one-step global reaction), computed with the pressure relaxation method (a) and LBGK method (b). Velocity of injection is equal to 10% of velocity of the oxidizer at the entrance.

The reaction is described by an one-step global reaction in the form

$$\alpha \text{ Fuel} + \beta \text{ Oxidizer} \rightarrow \text{Product}$$

with $\alpha = n/(n+1) = 1-\beta$ and $n = 10$. The production rate is given by $w_p/\rho_{mix} = \xi_F \cdot \xi_O \cdot \exp(-T_A/T) \cdot Da$, where the parameters are $T_A = 12$ and $Da = 620$. The heat production rate is assumed to be $4w_p/\rho_{mix}$. The additional parameters of these computations are $Pr = 0.7148$, $Sc = 1$, and $\mu \sim \sqrt{T}$. The lowest and highest values of the temperature for the both solutions are shown in brackets. The solution of the flow with the LBGK method requires 80% of CPU time necessary for the pressure relaxation method.

The agreement between the solutions obtained with the different numerical schemes was found to be excellent.

7.2. Numerical examples. A number of computational examples for reactive flows are performed with the LBGK method to demonstrate the capability of the method to deal with flows at relatively high Reynolds and Damköhler numbers. The use of refined, embedded grids is found to be absolutely necessary for such kind of anisotropic flow cases.

The flow of hot oxidizer through the periodical grid of porous burners is considered again. From the surfaces of the burners diffusional mass flux of the cold fuel is assumed. The chemistry is described with an one-step global reaction different from that above

$$\text{Fuel} + \text{Oxidizer} \rightarrow 2\text{Product}$$

with the production rate $w_p/\rho_{mix} = T\xi_F \cdot \xi_O \cdot \exp(-T_A/T) \cdot Da$, where the parameters are $T_A = 12$ and heat production rate is $4w_p/\rho_{mix}$. The other parameters are $Pr = 0.7148$, $Sc = 1$, $\mu \sim \sqrt{T}$. The Damköhler number defined as the ratio between the time of convection within one coarse cell and the characteristic time of chemical reaction is 1000. If the characteristic time of convection is related to the diameter of the cylinder then it corresponds to $Da = 15000$.

An embedded grid with refinement n is applied around the burner to resolve accurately boundary layers and thin zones of reaction. At first the case $Re = 100$, $n = 3$ is considered. Velocity at the entrance is $U_{ent} = 0.07c_0$ and the relaxation parameters on the coarse and fine grids at $T = 1$ are $\omega_c = 1.881$, $\omega_f = 1.682$ accordingly.

In Fig. 4 the picture of steady-state flow in the periodical cell at $Re = 100$, $n = 3$ is represented. Figure 4a shows the basic numerical mesh and embedded grid around the burner. In Figs. 4b and 4c the isolines of temperature and mass fraction of the product are plotted. Maximal values are $T_{max} = 3.01$, $\xi_{P,max} = 0.98$.

In Fig. 5 an enlarged part of the same flow in the vicinity of the burner is shown. Streamlines and temperature field are given in Fig. 5a, and the reaction rate in Fig. 5b. Recirculation zones behind the burners exist for these Reynolds and Damköhler numbers. Reaction occurs in the thin layer surrounding the burner, mainly in the front part of the burner. The strong anisotropy of the flow and the necessity of the use of embedded grids becomes clear from Fig. 5.

In Figs. 6 and 7 the flow of the same components through the same geometry is shown, but with higher *Re* number, $Re = 300$. An embedded grid with parameter of refinement 6 is applied around the burner. Velocity at the entrance is $U_{ent} = 0.1c_0$ and relaxation parameters on the coarse and fine grids at $T = 1$ are $\omega_c = 1.942$ and $\omega_f = 1.695$ accordingly.

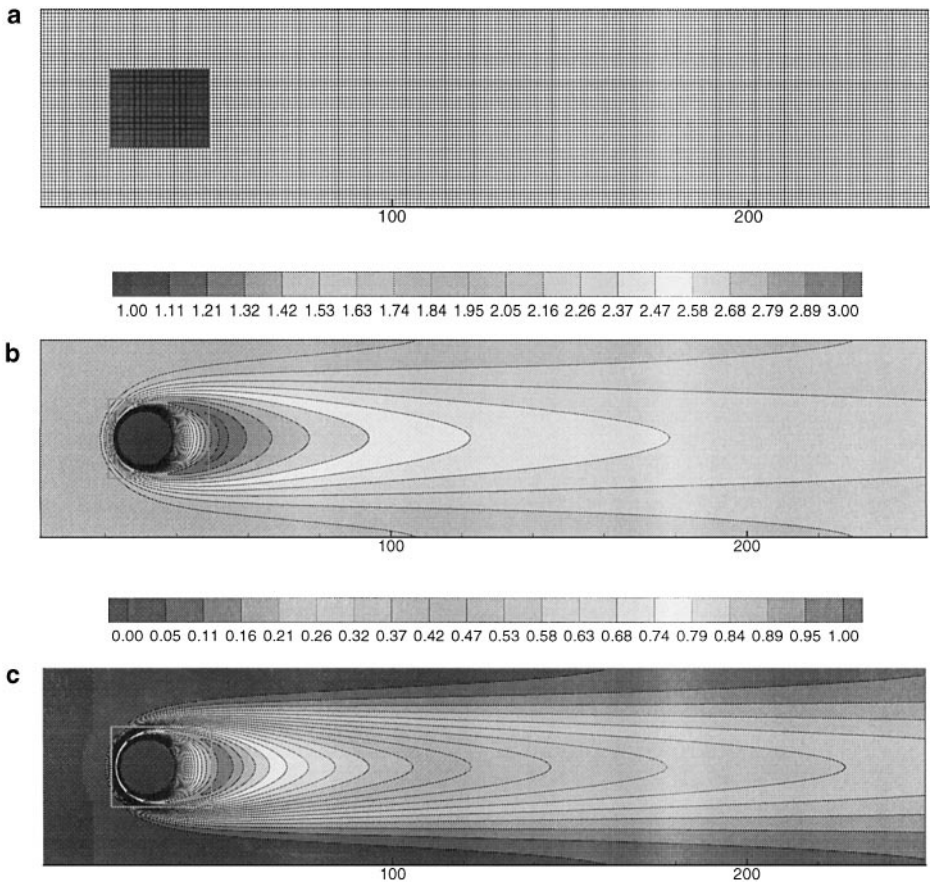

FIG. 4. Flow of the hot oxidizer through periodical grid of porous burners at Re = 100 (one-step global reaction). (a) Basic coarse grid and embedded grid ($n = 3$) around the porous burner; (b) temperature field; (c) mass fraction of the product.

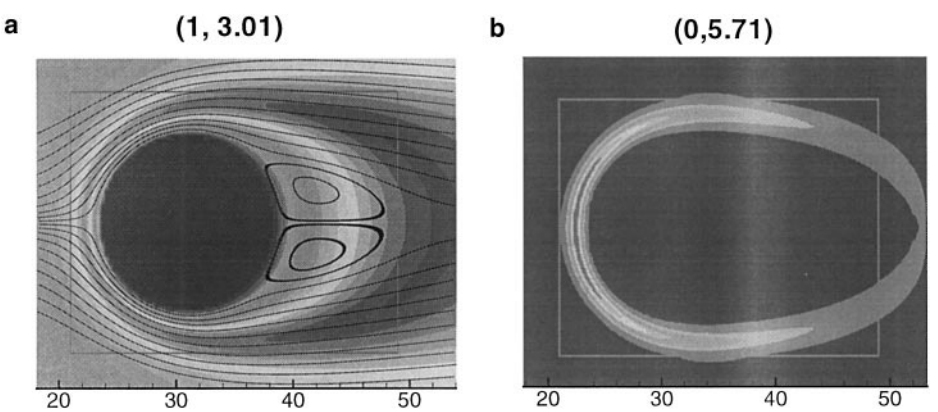

FIG. 5. Part of the flow of the hot oxidizer through periodical grid of porous burners at Re = 100 on the embedded grid, $n = 3$. (a) Temperature field and streamlines; (b) reaction rate.

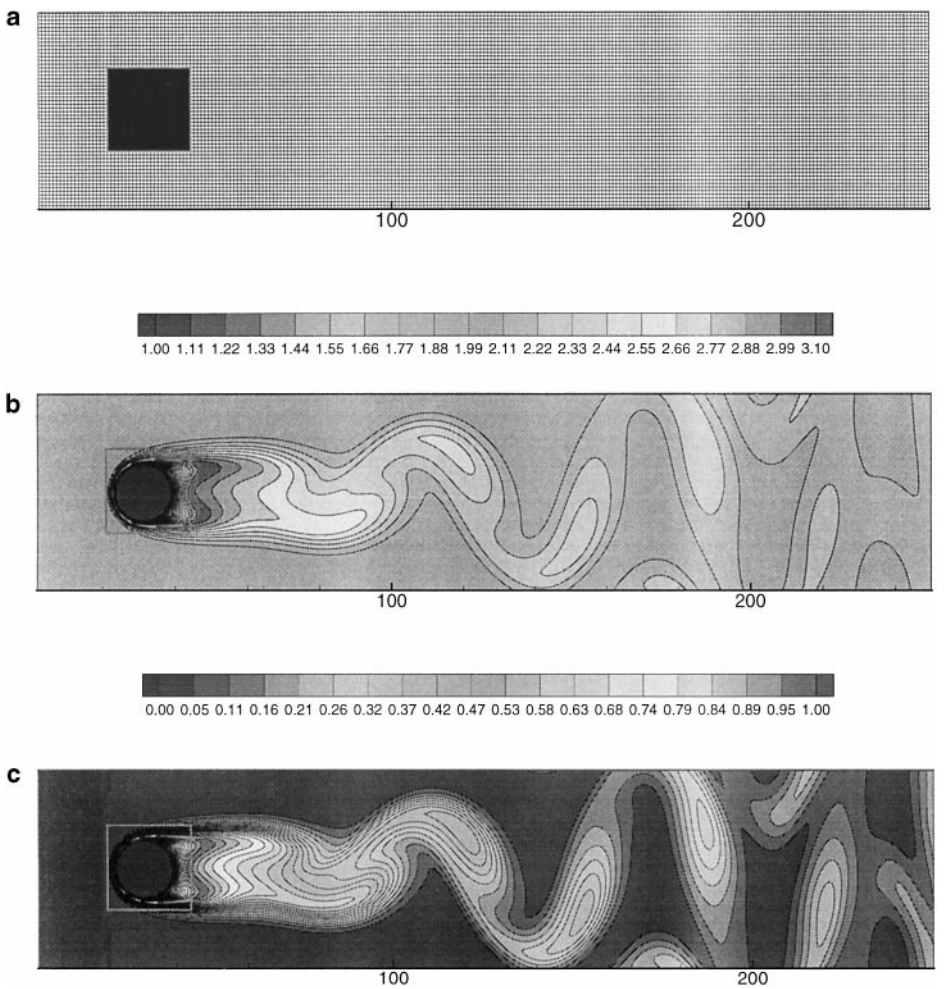

FIG. 6. Flow of the hot oxidizer through periodical grid of porous burners at Re = 300 (one-step global reaction). (a) Basic coarse grid and embedded grid ($n = 6$) around the porous burner; (b) temperature field; (c) mass fraction of the product.

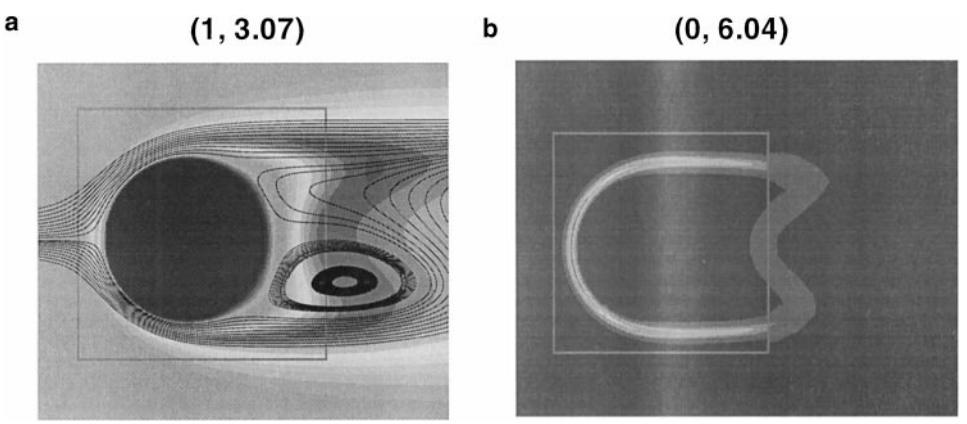

FIG. 7. Part of the flow of the hot oxidizer through periodical grid of porous burners at Re = 300 on the embedded grid, $n = 6$. (a) Temperature field and streamlines; (b) reaction rate.

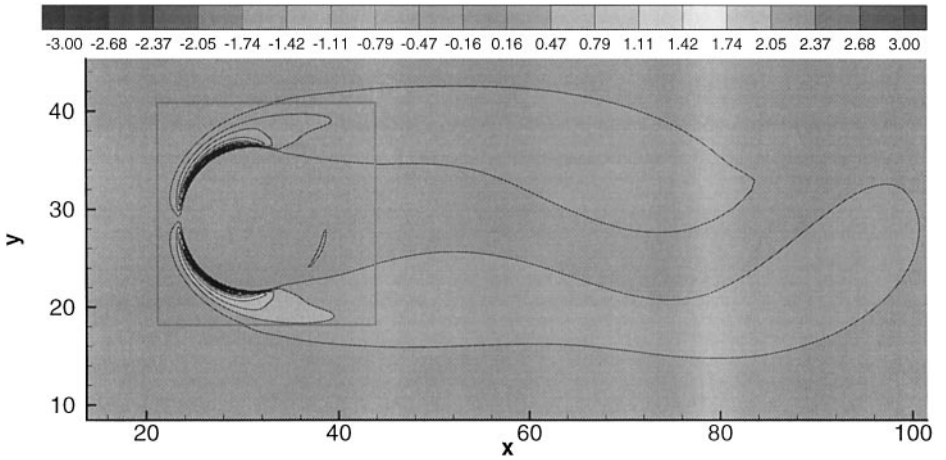

FIG. 8. Flow of the hot oxidizer through periodical grid of porous burners at Re = 300 (one-step global reaction). Instantaneous isolines of vorticity in the vicinity of the burner.

As it could be supposed in this case a time-periodic vortex street appears. Figure 6a shows the basic numerical mesh and embedded grid ($n = 6$) around the burner. In Figs. 6b and 6c the isolines of temperature and mass fraction of the product are plotted. In Fig. 7 the enlarged part of the same flow in the vicinity of the burner is shown. Streamlines and temperature field are given in Fig. 7a, and the reaction rate in Fig. 7b. As one can see from Fig. 6 the typical for vortex streets field of passive scalars as temperature and mass fraction of product outside of the zone of reaction appeared. The zone of reaction is divided in two parts: the stable one in which mainly reactions occur in the front part of the burner and the slightly oscillating one behind the burner in the region where vortices are induced.

To show the quality of this relatively sharp grid refinement instantaneous isolines of vorticity crossing the interface between two grid are presented in Fig. 8.

In Fig. 9 the oscillations of temperature and streamwise component of the mixture flux versus time are shown in the center point of the computational domain to justify once more our basic statement that on the late stage of computations with LBGK scheme the acoustic part of the solution is filtered out.

Here some important properties of the local grid refinement concept have to be pointed out. Consider some hypothetical uniform fine grid (FG) covering the whole computational domain and providing the same resolution in the zones where it is necessary as the embedded grid used in the previous simulations (Figs. 4, 5). The number of grid nodes used in the numerical simulation with embedded grid is equal to 16% of the number of grid nodes of FG, whereas the number of operation in the LBGK scheme for the same physical time interval on the uniform grid FG would be about 11 times larger. This win in the simulations using embedded grids is achieved due to the different time stepping in the zones of fine and coarse grids. Here one must also mention that this property was not used in the comparison of the performance with the pressure relaxation method as far as in both methods the flow was solved on the uniform Cartesian grids.

The next problems to be addressed in the future are the implementation of a detailed chemistry mechanism in the solver and the consideration of three-dimensional problems. The splitting of the numerical scheme into two parts, the LBGK part and the convective-diffusion part, allows us to increase easily the number of transport equations for species. Simple extension to three dimensions is one of the well-known advantages of LBGK modelling.

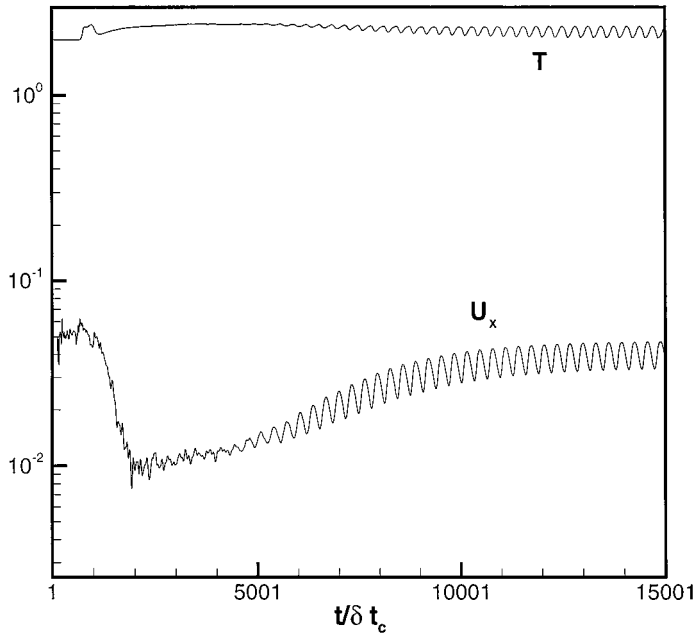

FIG. 9. Flow of the hot oxidizer through periodical grid of porous burners at Re = 300 (one-step global reaction). Oscillations of the temperature and streamwise mixture flux in the centre point of the computational domain.

8. CONCLUSION

The LBGK model, originally developed for simulating incompressible flows, was extended to flows at low Mach numbers, but variable densities. Algorithmic extensions, like local grid refinement and boundary fitting formulation, were adopted from previous studies to the new method. Analysis and numerical studies confirmed an accuracy of second order in space and time with respect to the lattice Knudsen number. The method preserves the advantages of the lattice BGK concept, as they are easy parallelization and flexible treatment of complex geometries, and results therefore in an accurate and efficient solution concept of low Mach number flows with variable density caused by temperature changes due to heat transfer or chemical reactions.

In the present paper a coupled solution procedure is presented, where the LBGK method for the flow computation is coupled with a finite-difference method for calculating temperature and species of a chemical reacting flow. The flows around porous burners were chosen for validating and testing the new scheme. Comparisons with the solutions obtained with a pressure-relaxation scheme for low Mach number approximation of the Navier–Stokes equations have shown the excellent agreement. Further studies of reactive flows in a wide regions of Reynolds and Damköhler numbers are presented.

APPENDIX

Analysis of the LBGK Method for LMNA

The proof of consistency and estimation of accuracy of the LBGK method for the solution of LMNA is based on a consideration of orders of magnitude in the two parameters, the

lattice Knudsen number ϵ, and the global Mach number M_g

$$\epsilon = \frac{\delta_x}{L} = \frac{c_0\,\delta_t}{L} \ll 1 \qquad \text{and} \qquad M_g = \frac{U_0}{c_0} \ll 1.$$

In the frame of molecular level, on which the LBGK method is numerically solved, the following non-dimensional variables related to c_0 and L are introduced:

$$\bar{x} = \frac{x}{L}, \quad \bar{t} = \frac{t}{L/c_0}, \quad \bar{c}_{pi} = \frac{c_{pi}}{c_0}, \quad \bar{c}_s = \frac{c_s}{c_0} = \frac{1}{\sqrt{3}}, \quad \bar{\delta}_x = \frac{\delta_x}{L} = \bar{\delta}_t = \frac{\delta_t}{L/c_0} = \epsilon. \quad (23)$$

The macroscopic variables are related to the following reference quantities:

$$\bar{\rho}_{mix} = \frac{\rho_{mix}}{\rho_0}, \quad \bar{T} = \frac{T}{T_0}, \quad \bar{a} = \frac{a}{a_0}, \quad \bar{u} = \frac{u}{c_0}, \quad \bar{P} = \frac{P}{\rho_0\, c_0^2}, \quad \bar{\nu} = \frac{\nu}{c_0\, L}. \quad (24)$$

In the following the bar-superscripts are skipped for simplicity. The modified LBGK equation, Eqs. (12) and (13), reads in non-dimensional form

$$f_{pi}(t+\epsilon, \mathbf{r} + \mathbf{c}_{pi}\epsilon) = f_{pi}(t, \mathbf{r}) + \omega\big[f_{pi}^{\mathrm{eq}}(t, \mathbf{r}) - f_{pi}(t, \mathbf{r})\big] - G(t, \mathbf{r}). \quad (25)$$

The function $G(t, \mathbf{r})$ is defined as

$$G(t, \mathbf{r}) = \rho_{mix}(t, \mathbf{r}) - \rho_{mix}(t - \epsilon, \mathbf{r}) \qquad \text{if } p = 0 \text{ and } G(t, \mathbf{r}) = 0 \quad \text{if } p \neq 0.$$

The effective equilibrium distribution function, Eq. (14), reads in non-dimensional variables

$$f_{pi}^{\mathrm{eq}} = t_p \left[\frac{P}{c_s^2} + \frac{\rho_{mix} u_\alpha c_{pi\alpha}}{c_s^2} + \frac{\rho_{mix} u_\alpha u_\beta}{2c_s^2} \left(\frac{c_{pi\alpha} c_{pi\beta}}{c_s^2} - \delta_{\alpha\beta} \right) + \frac{\nu u_\gamma \partial_\delta \rho_{mix}}{c_s^2} \left(\frac{c_{pi\gamma} c_{pi\delta}}{c_s^2} - \delta_{\gamma\delta} \right) \right] \quad (26)$$

with the definition of the dimensionless kinematic viscosity ν,

$$\nu = \frac{\epsilon}{6} \left(\frac{2}{\omega} - 1 \right). \quad (27)$$

Under the assumption of continuous physical space $(t, \mathbf{r})$ in the limit of $\epsilon \to 0$, the LBGK equation Eq. (25) is expanded in Taylor series with respect to small ϵ

$$\epsilon \left[\frac{\partial}{\partial t} + c_{pi\alpha} \frac{\partial}{\partial x_\alpha} \right] f_{pi} + \frac{\epsilon^2}{2} \left[\frac{\partial}{\partial t} + c_{pi\alpha} \frac{\partial}{\partial x_\alpha} \right]^2 f_{pi} + \omega\big[f_{pi} - f_{pi}^{eq}\big] = O(\epsilon^3) \quad (28)$$

and correspondingly the function $G(t, \mathbf{r})$,

$$G(t, \mathbf{r}) = \epsilon \partial_t \rho_{mix}(t, \mathbf{r}) - \frac{1}{2} \epsilon^2 \partial_t \partial_t \rho_{mix}(t, \mathbf{r}) + O(\epsilon^3).$$

The non-equilibrium distribution function is expanded for small deviations from the local equilibrium in the sense of a Chapman–Enskog expansion to

$$f_{pi} = f_{pi}^{\mathrm{eq}} + \epsilon f_{pi}^{(1)}. \quad (29)$$

The moments of the perturbation function $f_{pi}^{(1)}$ satisfy

$$\sum_{p,i} f_{pi}^{(1)} = 0, \qquad \sum_{p,i} f_{pi}^{(1)} c_{pi\alpha} = 0. \tag{30}$$

Introduction of the expansion Eq. (29) into the Taylor series Eq. (28) and sorting in orders of ϵ result in an expression for the perturbation function $f_{pi}^{(1)}$,

$$f_{pi}^{(1)}(t, \mathbf{r}) = -\frac{1}{\omega}\left(\frac{\partial f_{pi}^{\mathrm{eq}}(t, \mathbf{r})}{\partial t} + \frac{\partial f_{pi}^{\mathrm{eq}}(t, \mathbf{r})}{\partial x_\alpha} c_{pi\alpha}\right) + O\left(\epsilon f_{pi,tt}^{\mathrm{eq}}, \epsilon f_{pi,tx}^{\mathrm{eq}}, \epsilon f_{pi,xx}^{\mathrm{eq}}\right). \tag{31}$$

Summation over all discrete velocities in series Eq. (28) with Eq. (29) and Eq. (31) yields the equation of the zeroth moment

$$\partial_t \sum_{p,i} f_{pi} + \partial_\beta \sum_{p,i} f_{pi} c_{pi\beta} + \frac{1}{2}\epsilon\left(\partial_t \partial_t \sum_{p,i} f_{pi} + 2\partial_t \partial_\beta \sum_{p,i} f_{pi} c_{pi\beta} + \partial_\beta \partial_\gamma \sum_{p,i} f_{pi}^{\mathrm{eq}} c_{pi\beta} c_{pi\gamma}\right)$$
$$+ \partial_t \rho_{mix} - \frac{1}{2}\epsilon \partial_t \partial_t \rho_{mix} = O(\epsilon^2)$$

and of the first moments by multiplying with $c_{pi\alpha}$

$$\partial_t \sum_{p,i} f_{pi} c_{pi\alpha} + \partial_\beta \sum_{p,i} f_{pi}^{\mathrm{eq}} c_{pi\alpha} c_{pi\beta} + \frac{1}{2}\epsilon\left(\partial_t \partial_t \sum_{p,i} f_{pi}^{\mathrm{eq}} c_{pi\alpha} + 2\partial_t \partial_\beta \sum_{p,i} f_{pi}^{\mathrm{eq}} c_{pi\alpha} c_{pi\beta}\right.$$
$$\left. + \partial_\beta\left(1 - \frac{2}{\omega}\right)\partial_\gamma \sum_{p,i} f_{pi}^{\mathrm{eq}} c_{pi\alpha} c_{pi\beta} c_{pi\gamma}\right) = O(\epsilon^2).$$

Using symmetry properties of the lattice

$$\sum_{p,i} t_p c_{pi\alpha} = 0, \qquad \sum_{p,i} t_p c_{pi\alpha} c_{pi\beta} c_{pi\gamma} = 0, \qquad \sum_{p,i} t_p c_{pi\alpha} c_{pi\beta} c_{pi\gamma} c_{pi\delta} c_{pi\xi} = 0$$
$$\sum_{p,i} t_p c_{pi\alpha} c_{pi\beta} = c_s^2 \delta_{\alpha\beta}, \qquad \sum_{p,i} t_p c_{pi\alpha} c_{pi\beta} c_{pi\gamma} c_{pi\delta} = c_s^4 (\delta_{\alpha\beta}\delta_{\gamma\delta} + \delta_{\alpha\gamma}\delta_{\beta\delta} + \delta_{\alpha\delta}\delta_{\beta\gamma})$$

and the expression for effective equilibrium distribution function Eq. (26) one can obtain the following macrodynamical equations

$$\partial_t\left(\rho_{mix} + P/c_s^2\right) + \partial_\alpha \rho_{mix} u_\alpha$$
$$+ \frac{1}{2}\epsilon\left(\partial_t \partial_t\left(P - \rho c_s^2\right)/c_s^2 + 2\partial_t \partial_\alpha \rho_{mix} u_\alpha + \partial_\alpha \partial_\beta (\rho_{mix} u_\alpha u_\beta + P\delta_{\alpha\beta})\right) = O(\epsilon^2) \tag{32}$$

$$\partial_t \rho_{mix} u_\alpha + \partial_\beta (\rho_{mix} u_\alpha u_\beta + P\delta_{\alpha\beta})$$
$$= \partial_\beta \nu(\partial_\beta \rho_{mix} u_\alpha + \partial_\alpha \rho_{mix} u_\beta + \delta_{\alpha\beta}\partial_\gamma \rho_{mix} u_\gamma - u_\gamma \partial_\delta \rho_{mix}(\delta_{\alpha\gamma}\delta_{\beta\delta} + \delta_{\alpha\delta}\delta_{\beta\gamma}))$$
$$+ \epsilon\left(\frac{1}{2}\partial_t \partial_t \rho_{mix} u_\alpha + \left(1 - \frac{1}{\omega}\right)\partial_t \partial_\beta (\rho_{mix}\, u_\alpha u_\beta + P\delta_{\alpha\beta})\right) + O(\epsilon^2). \tag{33}$$

The terms on the right hand side, containing the viscosity ν, do not agree with the correct stress terms of the Navier–Stokes equations. However, the function P, still undefined, can

be used to cancel out the wrong terms included in Eq. (33). Comparing the terms of zero order with the required physical stress term, the function P has to be defined as

$$P = p^{(1)} + \frac{2}{3}\frac{\mu}{\rho_0}\partial_\gamma u_\gamma + \nu\partial_\gamma \rho_{mix} u_\gamma = c_s^2 \sum_{p,i} f_{pi}. \tag{34}$$

The function P, Eq. (34), is defined now as a function of the dynamic pressure $p^{(1)}$ and the divergences of the velocity and of the mixture flux. This definition is similar to the redefinition of pressure in turbulent modelling where the isotropic part of the stress tensor is added to the value of the dynamic pressure. Although in the internal points of the computational domain different terms included in function P do not have to be defined explicitly, all terms in P have to be introduced by discretizations at the boundaries of computational domain.

Using the definition of P the first moment Eq. (33) corresponds to the momentum equation in the form

$$\begin{aligned}
&\partial_t \rho_{mix} u_\alpha + \partial_\beta \left(\rho_{mix} u_\alpha u_\beta + p^{(1)}\delta_{\alpha\beta}\right) \\
&\quad = \partial_\beta\, \nu\rho_{mix}\left(\partial_\beta u_\alpha + \partial_\alpha u_\beta - \frac{2}{3}\delta_{\alpha\beta}\partial_\gamma u_\gamma\right) \\
&\qquad + \epsilon\left(\frac{1}{2}\partial_t\partial_t \rho_{mix} u_\alpha + \left(1 - \frac{1}{\omega}\right)\partial_t\partial_\beta(\rho_{mix} u_\alpha u_\beta + P\delta_{\alpha\beta})\right) + O(\epsilon^2).
\end{aligned} \tag{35}$$

The system of equations Eq. (32) with Eq. (34) and Eq. (35) corresponds to the continuity equation and the momentum equations of the LMNA of the Navier–Stokes equations beside the time derivative of P in the continuity equation and the terms proportional to ϵ in both equations.

These additional terms become on the order of the truncation error in the low frequency limit. As it was mentioned in Section 3, acoustic components of the solution dissipate in the transitional stage of computations relatively fast if no high frequency disturbances are generated by boundary conditions. After this dissipation the time advance of the LBGK scheme reproduces the low frequency solution only, which corresponds to Strouhal numbers of $Str = L_0/U_0 T = \delta_t/T M_g \epsilon \sim O(1)$. This time behaviour is typical for laminar vortical flows, as, e.g., for von Karman vortex streets, and was checked by computations.

For the proof of consistency of macrodynamical equations provided by the LBGK scheme the system of equations Eq. (32) and Eq. (35) in molecular scales is transformed to the characteristic scales of the low frequency solutions.

For re-normalizing the dimensionless variables, given in molecular scales Eq. (23) and Eq. (24) to the scales of the low frequency flows, new reference quantities L, U_0, μ_0, ρ_0 are introduced. The Mach number $M_g = U_0/c_0 \ll 1$ appears then as an additional parameter of magnitude.

The relationship between the dimensionless quantities in Eq. (23) and Eq. (24) (with bar-superscript) and the new dimensionless quantities (with tilde-superscript) is given by

$$\tilde{x} = \frac{x}{L} = \bar{x}, \qquad \delta\tilde{x} = \delta\bar{x} = \epsilon, \qquad \tilde{t} = \frac{t}{T} = \frac{t}{L_0/(UStr)} = \bar{t}\, M_g Str,$$

$$\delta\tilde{t} = \delta\bar{t} M_g Str = \epsilon M_g Str \qquad \tilde{\rho}_{mix} = \frac{\rho_{mix}}{\rho_0} = \bar{\rho}_{mix}, \qquad \tilde{u} = \frac{u}{U_0} = \frac{\bar{u}}{M_g},$$

$$\tilde{p}^{(1)} = \frac{p^{(1)}}{\rho_0 U_0^2} = \frac{\bar{p}^{(1)}}{M_g^2}, \qquad \tilde{P} = \frac{P}{\rho_0 U_0^2} = \frac{\bar{P}}{M_g^2} \qquad \tilde{\nu} = \frac{\nu}{\mu_0/\rho_0} = \bar{\nu}\frac{Re}{M_g}.$$

Using these transformations with the definition of the Reynolds number $Re = \rho_0 U_0 L/\mu_0$ and the time derivative $\partial_{\tilde{t}} = \partial_{\bar{t}}/(M_g Str)$ the following equations can be deduced from Eq. (32) and Eq. (35),

$$Str\partial_{\tilde{t}}\tilde{\rho}_{mix} + \partial_\alpha \tilde{\rho}_{mix}\tilde{u}_\alpha + StrM_g^2\partial_{\tilde{t}}\tilde{P}/c_s^2 = O(M_g\epsilon) \tag{36}$$

$$Str\partial_{\tilde{t}}\tilde{\rho}_{mix}\tilde{u}_\alpha + \partial_\beta \tilde{\rho}_{mix}\tilde{u}_\alpha\tilde{u}_\beta + \partial_\alpha \tilde{p}^{(1)} = \frac{1}{Re}\partial_\beta\left(\tilde{\mu}\left(\partial_\beta\tilde{u}_\alpha + \partial_\alpha\tilde{u}_\beta - \frac{2}{3}\delta_{\alpha\beta}\partial_\gamma\tilde{u}_\gamma\right)\right) + O(M_g\epsilon). \tag{37}$$

Assuming the Mach number M_g is on the order of ϵ^a, $a > 0$ the consistency with continuity and momentum equations of LMNA is proven. Moreover, macrodynamical equations of the LBGK scheme Eqs. (36), (37) approximate continuity and momentum equations of LMNA with the asymptotical accuracy of ϵ^2 when $\epsilon \to 0$, $M_g \sim \epsilon$.

Usually in the numerical simulations with the LBGK scheme one uses the following order of small but finite ϵ and M_g numbers: $M_g \sim \epsilon \sim 0.1$. In this case the previous asymptotic estimation of accuracy is not sufficient as far as in some regions of the flow (as, for example, in the zones of vortex shedding) the space deviations of mixture flux on the characteristic length can be two orders smaller than the reference value. One way to ensure the second order accuracy in ϵ of the scheme in the whole computational domain is the decreasing of global Mach number M_g which leads in the inverse increasing of the computational time and loss of the efficiency of the solver. The other way is the use of the following semi-empirical criteria $[P]^t \sim O([\rho_{mix}]^t, [P]^s), [\rho_{mix}u]^t \sim [\rho_{mix}u]^s$. Here notations $[F]^t$, $[F]^s$ are used for the local deviations of variable F on the characteristic time and length accordingly. These estimations are based on the assumption that in the absence of acoustic the local time-deviations of the dynamic part of the pressure and mixture flux are on the order of their local space deviations. These criteria can be easily checked during the computations. With these estimations one can obtain the following over-estimation for $[P]^s$ from the momentum equation $[P]^s \sim [\rho_{mix}u]^s$ which ensures that "wrong" terms in the continuity equation are on the order of $\epsilon^2[\rho_{mix}u]^s$ and Eqs. (36), (37) approximate the continuity and momentum equation of LMNA with second order accuracy in ϵ.

ACKNOWLEDGMENTS

We thank Irenäus Wlokas for his assistance in producing the finite difference simulations used as reference solutions in this paper. O.F. thanks Professor S. Succi, Professor V. S. Ryaben'kii, Dr. A. Povitsky, and Dr. L.-S. Luo for the useful discussions. This work has been supported by the DFG (German Research Society).

REFERENCES

1. B. T. Chu and L. S. G. Kovasznay, Non-linear interactions in a viscous heat-conducting compressible gas, *J. Fluid. Mech.* **3**, 494 (1958).
2. G. J. Sivashinsky, Hydrodynamics theory of flame propagation in an enclosed volume, *Acta Astronaut.* **6**, 631 (1979).
3. G. R. Rehm and H. R. Baum, The equations of motion for thermally driven flows, *J. Res. Natl. Bur. Standards* **83**(3), 297 (1978).

4. P. A. McMurtry, W. H. Jou, J. J. Riley, and R. W. Metcalfe, Direct numerical simulations of a reacting mixing layer with chemical heat release, *AIAA J.* **24** (1986).
5. A. J. Chorin, Numerical solution of the Navier–Stokes equations, *Math. Comput.* **23**, 341 (1968).
6. G. McNamara and G. Zanetti, Use of the Boltzmann equation to simulate lattice-gas automata, *Phys. Rev. Lett.* **61**, 2332 (1988).
7. F. Higuera, S. Succi, and R. Benzi, Lattice gas dynamics with enhanced collisions, *Europhys. Lett*. **9**, 345 (1989).
8. Y. H. Qian, D. d'Humieres, and P. Lallemand, Lattice BGK models for Navier–Stokes equation, *Europhys. Lett.* **17**(6), 479 (1992).
9. S. Chen, Z. Wang, X. Shan, and G. D. Doolen, Lattice BGK models for Navier–Stokes equation, *J. Statist. Phys.* **68**, 379 (1992).
10. Q. Zou, S. Hou, S. Chen, and G. Doolen, An improved incompressible lattice Boltzmann model for time-independent flows, *J. Statist. Phys.* **81**, 35 (1995).
11. X. He and L.-S. Luo, Lattice Boltzmann model for the incompressible Navier–Stokes equation, *J. Statist. Phys.* **88**, 927 (1997).
12. O. Filippova and D. Hänel, Grid refinement for lattice-BGK models, *J. Comput. Phys.* **147**, 219 (1998).
13. O. Filippova and D. Hänel, Acceleration of lattice-BGK scheme with grid refinement, *J. Comput. Phys.*, in press.
14. S. Succi, G. Bella, and F. Papetti, Lattice kinetic theory for numerical combustion, *J. Sci. Comput.* **12**(4), 395 (1997).
15. O. Filippova and D. Hänel, Lattice–BGK model for low Mach number combustion, *Int. J. Mod. Phys. C* **9**(8), (1998).
16. S. Chen and G. D. Doolen, Lattice Boltzmann method for fluid flows, *Annu. Rev. Fluid Mech.* **30**, 329 (1998).
17. X. He and G. Doolen, Lattice Boltzmann method on curvilinear coordinate system: Vortex shedding behind a circular cylinder, *Phys. Rev. E* **56**(1), 434 (1997).
18. O. Filippova and D. Hänel, Lattice-Boltzmann simulation of gas-particle flow in filters, *Comput. & Fluids* **26**(7), 697 (1997).
19. R. Mei, private communication, 1999.
20. R. Mei, L.-S. Luo, and W. Shyy, An accurate curved boundary treatment in the lattice Boltzmann method, *J. Comput. Phys.* **155**, 307 (1999).
21. V. S. Ryaben'kii, private communication, 1999.
22. E. S. Oran and J. P. Boris, Numerical Simulation of Reactive flow (Elsevier, Amsterdam/New York, 1987).
23. A. G. Tomboulides, J. C. Y. Lee, and S. A. Orszag, Numerical simulation of low Mach number reactive flows, *J. Sci. Comput.* **12**(2), 139 (1997).
24. A. G. Tomboulides and S. A. Orszag, A quasi-two-dimensional benchmark problem for low Mach number compressible codes, *J. Comput. Phys.* **146**, 691 (1998).
25. M. D. Smooke, R. E. Mitchell, and D. E. Keues, Numerical solution of two-dimensional axisymmetric laminar diffusion flames, *Combust. Sci. Tech.* **67**, 85 (1989).
26. O. Filippova and D. Hänel, A novel numerical scheme for reactive flows at low Mach number, in *Proc. of LGA99, Tokyo, Japan*, in press.